AIAA-95-

DEVELOPMENT OF A POLYMERIC PIEZOELECTRIC C-BLOCK ACTUATOR USING A HYBRID OPTIMIZATION TECHNIQUE

Charles E. Seeley†
Aditi Chattopadhyay††

Department of Mechanical and Aerospace Engineering
Arizona State University
Tempe, AZ, 85287

Diann Brei*
Department of Mechanical Engineering and Applied Mechanics
University of Michigan
2250 G. G. Brown
Ann Arbor, MI, 48109

Abstract

A new class of polymeric piezoelectric bimorph actuators, called C-blocks because of their curved shape, has been developed to overcome limitations of conventional bimorph and stack piezoelectric configurations. A hybrid optimization procedure has been developed for efficient implementation of these actuators. The procedure developed is used to investigate design trade-offs associated with various performance criteria such as maximum deflection, force and strain energy. The set of design variables to optimize the C-block actuators, which can be used alone or can be combined in series and/or parallel, includes both continuous and discrete parameters. This necessitates the development of a hybrid optimization technique. The results of the optimization procedure indicate useful trends in the design variables for the efficient implementation of these actuators.

2. Nomenclature

a, z	continuous, discrete variables
b	width
d_{31}	piezoelectric coefficient
f	objective function
F_{KS}	composite objective function
g	constraint
h	height
l	length
M	moment
P	applied force
p_{nu}	number of units in parallel
r	radius from center of curvature
r_n	radius from neutral axis
S	search direction
s_{nu}	number of units in series
T	temperature
t	layer thickness
U*	strain energy
v	applied voltage
Y	Young's modulus
z	distance to midplane
α	step size
ρ	drawdown factor
Φ	design variable vector

subscripts

b	bonding layer
e	electrode layer
p	piezoelectric layer
tot	total structure
max	maximum value

3. Introduction

Smart materials have recently found widespread applications in vibration control. The applications range from large flexible space structures[1], fixed wing[2] and rotary wing aircraft[3,4] to automotive suspensions[5]. Piezoelectric materials are popular as actuators because they are light, fast and have low power consumption. They also have a large bandwidth and a relatively large induced strain for an applied voltage[6]. However, the bimorph and stack configurations most commonly used have limitations insofar as the stack configuration does not produce large deflections and the bimorph configuration supplies only a low force.

A new class of piezoelectric actuators has been developed that demonstrates better force and deflection capabilities[7,8]. These actuators, called C-blocks because of their half circle shape, can produce approximately five times the force of the traditional bimorph design with only a slight decrease in deflection[7]. In addition, C-blocks can be combined in series or in parallel like building blocks to form larger actuator architectures that provide improved deflection or force capabilities, respectively[7,8]. Because they can be combined, extra

---

† Graduate Research Assistant, Student Member AIAA

†† Associate Professor, Senior Member AIAA, Member SPIE, ASME, AHS, ISSMO, AAM

* Assistant Professor, Member SPIE, ASME

design freedoms are gained which create many feasible design options for actuator configurations. With so many alternatives to choose from, selection of the optimal material, geometric and combinatorial parameters for a given application can be difficult. Optimization techniques must be developed to aid in this selection process.

Conventional optimization techniques can be divided into two distinct categories. The first, gradient based search methods[9], rely on gradient information of the objective function and constraints to direct continuous design variables, such as thicknesses or material properties, to improve the objective function. The second category uses combinatorial techniques with discrete design variables, such as number of plies or actuator locations, to improve the objective function. Probabilistic methods [10,11] are often employed in discrete problems to search for a more global optimum, although often at additional computational effort. An optimization problem which contains exclusively continuous or discrete design variables can be solved using the appropriate continuous or discrete technique. However, gradient based methods normally cannot be used to solve a discrete problem unless a continuous relaxation of the discrete variables is possible which may lead to a sub optimal solution due to rounding errors and the possible presence of local minima. Similarly, discrete techniques may be inappropriate for use with continuous problems. A thorough search of the literature revealed the lack of available methods to investigate engineering problems in which both continuous and discrete design variables are present. The design and optimization of C-block type actuators are associated with both continuous and discrete design variables. Therefore, it is necessary to use a hybrid optimization technique[12] which can accept both types of design variables.

In the current research, a model of the C-block actuators is developed which is extended by combining identical actuators in series or in parallel to improve performance. A hybrid optimization technique developed by Chattopadhyay and Seeley[12] is used which is based on a modified Simulated Annealing (SA) algorithm[13] and utilizes available gradient information to improve efficiency. The procedure is applied to the optimization of the C-block actuators to improve deflection, force and total work performance. The efficiency of the hybrid technique is also discussed.

4. Model development

The C-block actuators are constructed out of two curved piezoelectric layers in a bimorph configuration resulting in a half circle as shown in Fig. 1. The piezoelectric material is chosen to be Polyvinylidene Fluoride (PVDF) since piezoceramic materials are too brittle to withstand the necessary deformations required and are too awkward to form into unusual shapes. The piezoelectric layers are surrounded on both sides by an electrode layer of silver ink. The bonding layer consists of a common epoxy used to connect the two piezoelectric layers. These layers are actuated with equal but opposite electric fields to produce a bending moment which is used as the actuation mechanism. The equations for the C-block micoactuators have been developed for the most part in a previous work[7,8]. Note that a single C-block actuator is referred to as a *micro*actuator. When several C-block actuators are combined in series or in parallel, the entire configuration is called a *macro*actuator. The C-block microactuator is modeled as a general curved beam. A Bernoulli-Euler strain distribution is assumed instead of a uniform strain distribution since the ratio of total actuator thickness to the piezoelectric material thickness is small (less than five)[15]. An energy method is used to derive the deflection and force models of the C-block microactuator.

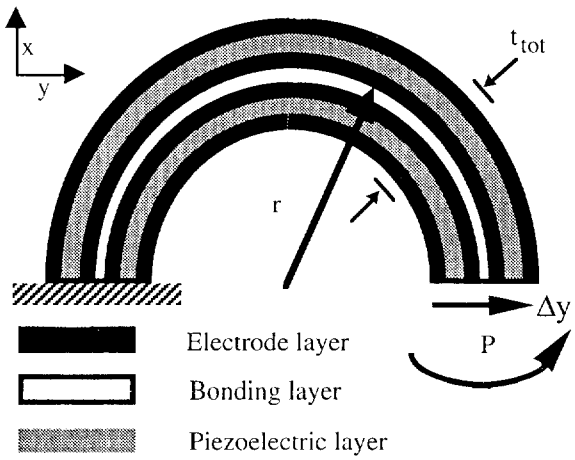

Figure 1. C-block microactuator.

The moment created by energizing the piezoelectric layer (M_e) is determined as follows[7].

$$M_e = Y_p d_{31} E_3 b_p (z_e^2 - z_p^2) \quad (1)$$

where Yp is the modulus of the piezoelectric layer, d_{31} is the piezoelectric coefficient, E_3 is the applied electric field, b_p is the width of the piezoelectric layer and z_e and z_p are the distances from the electrode and piezoelectric layers to the midplane, respectively. The strain energy U* can be calculated by deriving the strain energy in an element of volume and then integrating across all the layers of the microactuator and along the circumferential length.

$$U^* = \int \frac{M^2}{2(r - r_n) Y A_{tot}} d\phi \quad (2)$$

where M is the moment which includes M_e, the moment due to the piezoelectric actuation and the moment due to any external loads. The quantities r and r_n are the distances to the midplane and neutral axis, respectively and YA_{tot} represents the stiffness of the actuator. The

formulations of r_n and YA_{tot} are somewhat lengthy and can be found in Ref. 7. The deflection for a microactuator can be determined by using Castigliano's theorem. It is assumed that no external loads are applied so that M = M_e. By adjoining several microactuators in series, as shown in Fig. 2, and assuming that all of the C-block units are identical and are energized in the same manner, the total deflection can be written as follows.

$$\Delta_y = s_{nu} \frac{2M_e r}{YA_{tot}(r - r_n)} \tag{3}$$

where s_{nu} is the number of units connected in series. Similarly, by using several microactuators in parallel as indicated in Fig. 3, the induced force (P) from piezoelectric actuation can be calculated as follows.

$$P = -p_{nu} \frac{4M_e}{r\pi} \tag{4}$$

where p_{nu} is the number of actuators in parallel.

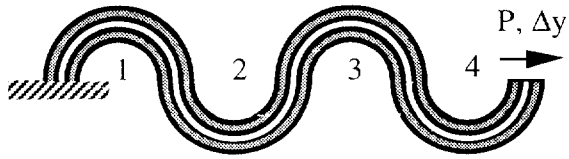

Figure 2. C-block actuators combined in series.

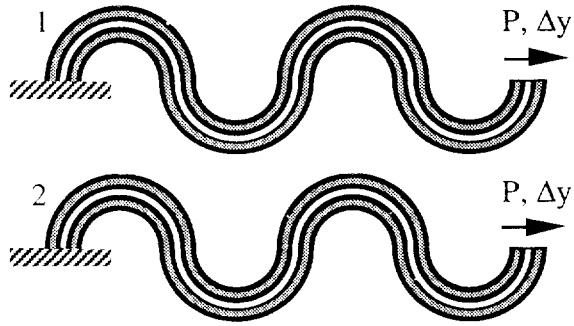

Figure 3. C-block actuators combined in series and in parallel.

Many applications of these macroactuators require a combination of both deflection and force. The most efficient representation of both the deflection and the force together is the work done by the actuator, or equivalently, the strain energy induced by piezoelectric actuation. By integrating Eqn. 2 and assuming that no external loads are applied, the strain energy (U*) for a macroactuator combined in both series and in parallel units is expressed as follows.

$$U^* = p_{nu} s_{nu} \frac{M_e^2 \pi}{2(r - r_n) YA_{tot}} \tag{5}$$

The deflection and force of the C-block actuators can be significantly increased by combining multiple units in series, parallel or both. However, several performance related issues are involved in the efficient design of the actuators. These can be addressed using formal optimization techniques. In this work, the nonlinear constrained optimization problem is converted to an unconstrained problem using a composite objective function. This function is then minimized using a hybrid optimization technique The optimization strategy is described next.

5. Optimization Formulation

5.1 Composite objective function

The general multiobjective optimization problem can be stated as follows.

Minimize	$f_k(\Phi)$	k = 1, 2,.., NOBJ
subject to	$g_n(\Phi)$	n = 1, 2, ., NCON

$$\Phi_L \le \Phi \le \Phi_U$$

where f_k is the kth objective function, g_n is the nth constraint and Φ is the design variable vector. The quantities NOBJ and NCON denote the number of objective functions and constraints and the subscripts L and U represent upper and lower bounds on the design variables, respectively.

The Kreisselmeier-Steinhauser (K-S) function approach is used to efficiently combine multiple and conflicting design objectives and constraints into a single composite function[16]. Recent studies have successfully demonstrated the usefulness of the K-S function technique in practical design problems[17]. In the K-S formulation, each original objective function is transformed into a reduced objective function $F_k(\Phi)$ as described in Ref 16. Since the reduced objective functions are analogous to constraints, a new constraint vector f_m is introduced where m = NCON + NOBJ and includes the reduced objective functions in addition to the original constraints. The new composite K-S objective function to be minimized is defined as follows.

$$F_{KS}(\Phi) = f_{max} + \frac{1}{\rho} \ln \sum_{i=1}^{m} e^{\rho(f_m(\Phi) - f_{max})} \tag{6}$$

where the quantity f_{max} represents the maximum violated constraint and the parameter ρ is analogous to the draw-down factor of penalty function formulations and controls the distance from the surface of the K-S envelope to the surface of the maximum constraint function. A larger value of ρ moves the K-S function envelope closer to the maximum violated constraint while a smaller value of ρ retains contributions from all of the objective functions and constraints. The K-S function is sensitive to both the original objective functions and any violated constraints.

The result is the best feasible compromise between all of the original objective functions and constraints.

5.2 Hybrid optimization

The design variable vector ϕ includes both continuous design variables (a_i) such as the piezoelectric layer thickness t_p and discrete design variables (z_j) such as the number of actuators in parallel (p_{nu}). Continuous design variables are not compatible with combinatorial optimization methods such as branch and bound techniques which require integer values to operate. Similarly, discrete variables are not compatible with gradient based optimization methods unless a continuous relaxation of the discrete variables is allowed which may lead to sub optimal solutions. The solution of optimization problems which contain both discrete and continuous design variables necessitates the development of a single technique which efficiently incorporates both types of design variables.

Simulated annealing has been shown to be an effective method for combinatorial optimization using discrete design variables[12,13,14,17,18]. The method works by repeatedly perturbing a current design a small amount. While better designs are always retained, worse designs are occasionally accepted under a given probability. This allows the algorithm to climb out of local minima while improving the objective function F which results in a more global solution. In a procedure developed by Chattopadhyay and Seeley (Ref. 12) the simulated annealing technique has been used in conjunction with a gradient based search. The result is a hybrid optimization technique which can efficiently include both continuous and discrete design variables. The algorithm is outlined below.

START
Current design is F
Select either continuous or discrete variable to perturb for F_{new}
  If continuous variable selected
    $a_{i_{new}} = a_i + \alpha S_i$
  Else if discrete variable selected
    $z_{j_{new}} = z_{jq}$
  End if
Compute F_{new}
If $F_{new} \leq F$ *then*
  $F = F_{new}$
Else if $P_{acc} \geq P$ *then*
  $F = F_{new}$
End if
Go to START

In the above algorithm, the quantity F is the current value of the K-S function F_{KS}, although any similar cost function is also appropriate here for a constrained nonlinear optimization problem. The continuous and discrete design variables are represented by a and z respectively and the subscript new denotes current perturbed design variables The quantity α is a random step size selected to be within some percentage of the current value of the continuous variables (e.g., $-1\% \leq \alpha \leq +1\%$) and S_i is the search direction which is determined from the gradient of the K-S composite objective function[16] for the current design variable. The continuous design variables are perturbed using the step size and the search direction to improve the efficiency of the search while the discrete variables are perturbed by randomly selecting specified values z_{jq} within a given range. These specified discrete values may be integers or decimal values such as common beam dimensions in a structural sizing problem. Move limits and bounds are imposed on the continuous design variables to ensure a physically meaningful design. The parameter P is a random number such that $0 \leq P \leq 1$ and the acceptance probability (P_{acc}) of retaining a worse design is computed as follows.

$$P_{acc} = e^{-\frac{\Delta F}{T}} \tag{7}$$

where ΔF represents the change in objective function and T is the "temperature" which is computed at each iteration using the following relation.

$$T = T_0 r^i \tag{8}$$

where the temperature T is reduced from the initial temperature T_0 for successive iterations i according to the cooling rate r[18]. A higher temperature allows worse designs to be occasionally accepted according to the given probability which allows the algorithm to climb out of possible local minima. The probability is reduced to zero during optimization so that only better designs are accepted to ensure smooth convergence.

The hybrid optimization procedure relies on a directed search for the continuous design variables which increases efficiency. However, the probabilistic nature of the simulated annealing algorithm allows the optimization procedure to climb out of local minima. Therefore, the procedure exhibits benefits of both gradient-based and discrete optimization techniques.

6. Results

6.1 Experimental Results

A variety of experiments are performed to validate the mathematical models for polymeric C-block actuators. For each of the experiments, the laboratory set up is similar. A high voltage supply is connected directly to a clamped C-block prototype (Fig. 4) for actuation. A three dimensional scale is used for deflection measurements. Force measurements are performed by hanging small aluminum weights from a loop of thread attached to the tip of the C-block.

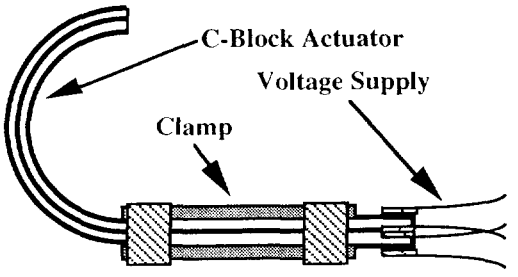

Figure 4. Final Clamped C-block Prototype

C-block prototypes are fabricated using a five step method. In the first step pre-electroded film is processed to create the desired electrode pattern. A plastic mask is secured to a prepoled Polyvinylidene Fluoride (PVDF) piezoelectric strip. The exposed electrode is etched away using Methyl Ethyl Keytone thus separating a solid electrode to form two electrodes. Each expanded electrode on a serial macroactuator mask corresponds to one C-block. Therefore, different masks are used to manufacture the C-blocks since a single a microactuator has only one electrode while a macro actuator has multiple electrodes.

In the second step, electrode wires are attached to the electrodes on the piezoelectric film. Because the film is so thin, electrode wires can not be directly soldered to the electrodes on the film. Therefore, electrode wires are indirectly attached to the PVDF film by soldering them to electrical adhesive tape and then attaching the tape to the film. Next, the two films are bonded together to create the bimorph structure of the C-block actuators. Epoxy is applied and rolled off one film using a micrometer mackrel. The mating film is aligned with the top of the epoxied film making sure that the polarity of both films are in the same direction.

Once the film is bonded together it, is placed in a mold system to generate the semi-circular shape of the C-block actuators or the regular repeating pattern of the serial macroactuator. This mold system consists of many dowels as shown in Figure 5. The number of dowels corresponds to the number of C-blocks used in the serial macroactuator. The film is wrapped around a set of dowels and the ends are secured. To compensate for material relaxation, an overwrapping technique is used. In this technique, the bimorph is wrapped past the half circle shape as depicted in Figure 6. It takes eight hours for the epoxy to set. The final step involves releasing the C-block actuator and rigidly supporting it by attaching the clamp which consists of two glass slides with tape as demonstrated in Figure 4 for a microactuator.

Once prototypes are fabricated, a set of experimental procedures are used to verify that the prototypes and the mathematical models developed agree. Three different types of experiments are performed, deflection-voltage, force-voltage and force-deflection. Each experiment is replicated with a wide variety of prototypes that differed in radii, layer thicknesses and the number of C-blocks used in combination. For each of these experiments, a prototype is clamped into the laboratory setup. The details of each experiment are presented next.

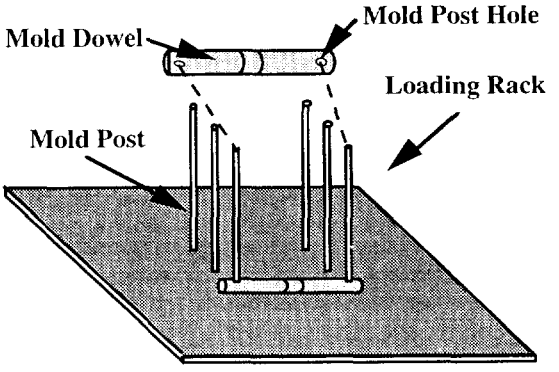

Figure 5. Fabrication mold dowel and loading rack.

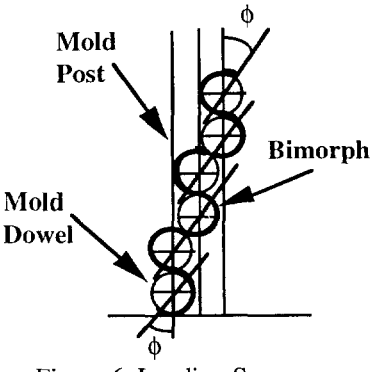

Figure 6. Loading Sequence.

6.1.1 Deflection-Voltage

The deflection-voltage experiments are used to test the maximum deflection generated by C-blocks for a given input voltage. In this experiment, a DC voltage is applied to the actuator in steps of 25 volts from zero to 325 volts. For each voltage increment, the coordinate of the tip is measured and the initial position is subtracted to determine the deflection.

The results for a representative C-block are shown in Fig. 7. The results for a representative serial macroactuator are shown in Fig. 8. The midplane radius and total thickness (Fig. 1) are indicated in the figure captions for each experiment. A least squares method is used to fit a linear regression line to the experimental data. For this case and all other cases as well, a statistical hypothesis test as outlined in Hines and Montgomery[20] is used to confirm, with a Type I error of only five percent, that there is no significant departure from the theoretical line and the regression line generated from experimental data collected. A Type I error is the probability that the null hypothesis will be rejected when it is true and should not be rejected. The results from all the experiments are within 10% of the predicted behavior for each set of radii

and thickness parameters and are validated using the hypothesis test. These results validate the quantitative models and prove that the deflection from individual C-blocks linearly add to accumulate into the deflection generated by a serial macroactuator. A curve for an equivalent PVDF straight bimorph is also presented in Fig. 7 which can be verified from Tzou's work[19]. From these results, it can be seen that the induced deflection for a single C-block actuator is slightly less than for a conventional bimorph actuator.

6.1.2 Force-Voltage Experiment

The force-voltage experiments are used to test the maximum force generated by C-blocks for a given input voltage. Again, a DC voltage is applied in 25 volt increments up to a maximum of 325 volts. For each voltage increment, the force is measured by adding weights to the thread loop until the tip deflection is zero. The results for a representative C-block are shown in Fig. 9 The experimental and theoretical results are in excellent agreement which validates the quantitative models. A representative PVDF straight bimorph is also presented in Fig. 9. It can be seen that the force generated by a basic C-block element is significantly higher than a conventional straight bimorph.

6.1.3 Force-Deflection Experiment

The force-deflection experiments are used to test the overall static performance of C-block actuators. A constant voltage of 325 volts is applied to a single C-block actuator and the tip deflection is determined. Weights in increments of 20 mg are then added to the thread loop. The tip deflection at each additional weight is also determined. This procedure is repeated until the deflection of the tip is zero. The results for a representative C-block are shown in Fig. 11. Once again, excellent agreement is observed between theory and experiment. The representative PVDF straight bimorph also presented in Fig. 11 indicates that C-blocks generate significantly larger force but less deflection than a straight bimorph. The effects of model parameters and trade-offs between the force and deflection are investigated using the hybrid optimization procedure and are described next.

6.2 Optimization results

The hybrid optimization procedure is implemented along with the macroactuator model developed to determine design trends for three different cases using three different design objectives. These design objectives include induced deflection, force and strain energy of the macroactuator due to activation of the piezoelectric material. The different cases studied are described next.

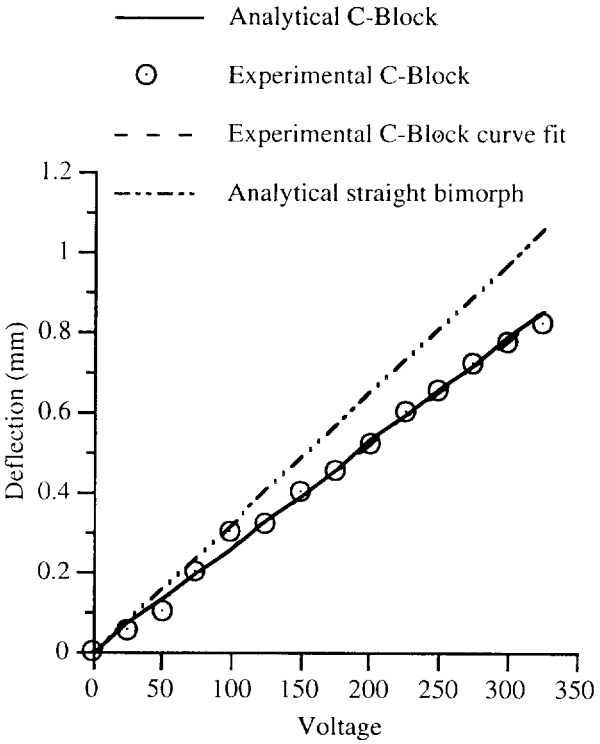

Figure 7. Single actuator; deflection versus voltage ($r = 1.37$ cm, $t_{tot} = 0.100$ mm).

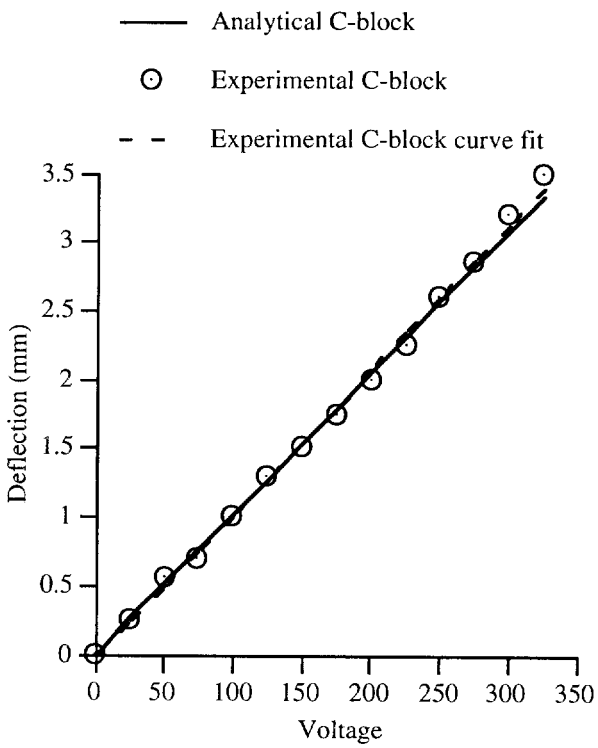

Figure 8. Series actuator; deflection versus voltage ($r = 1.39$ cm, $t_{tot} = 0.112$ mm).

Maximize:

Case 1:	deflection	(Δy)
Case 2:	force	(P)
Case 3:	strain energy	(U^*)

subject to:

$$g_1 = \frac{z_b}{r} - 1 \le 0$$

$$g_2 = \frac{z_e}{r} - 1 \le 0$$

$$g_3 = \frac{z_p}{r} - 1 \le 0$$

$$g_4 = \frac{z_{eo}}{r} - 1 \le 0$$

$$g_5 = \frac{t_{tol}}{r} - 1 \le 0$$

$$g_6 = \frac{r_n}{r} - 1 \le 0$$

$$g_7 = \frac{2}{h_{max}}\left[r + \frac{p_{num}\, t_{tol}}{2}\right] - 1 \le 0$$

$$g_8 = \frac{2 r s_{num}}{l_{max}} - 1 \le 0$$

$$g_9 = \frac{v}{v_{max}} - 1 \le 0$$

side constraints:

$$5 \le t_b \le 1000\ \mu m$$
$$0.6 \le t_e \le 20.0\ \mu m$$
$$8.0 \le t_p \le 1000.0\ \mu m$$
$$0.001 \le r \le 50.0\ mm$$

The optimization problem is formulated with four continuous design variables. The first three continuous design variables are the thicknesses of the bonding, electrode and piezoelectric layers represented by t_b, t_e and t_p, respectively. Additionally, the radius is included as a design variable and is denoted r. Two additional design variables, p_{nu} and s_{nu}, are discrete variables and represent the number of units in parallel and in series, respectively. The width of the microactuator is chosen to be 1 cm for convenience. All other parameters describing the macroactuator model are either previously specified depending on the case investigated, or can be determined from the six independent design variables.

The first four constraints (g_1-g_4) are imposed to ensure that the distance from any layer to the midplane is less than or equal to the radius. The fifth constraint, g_5,

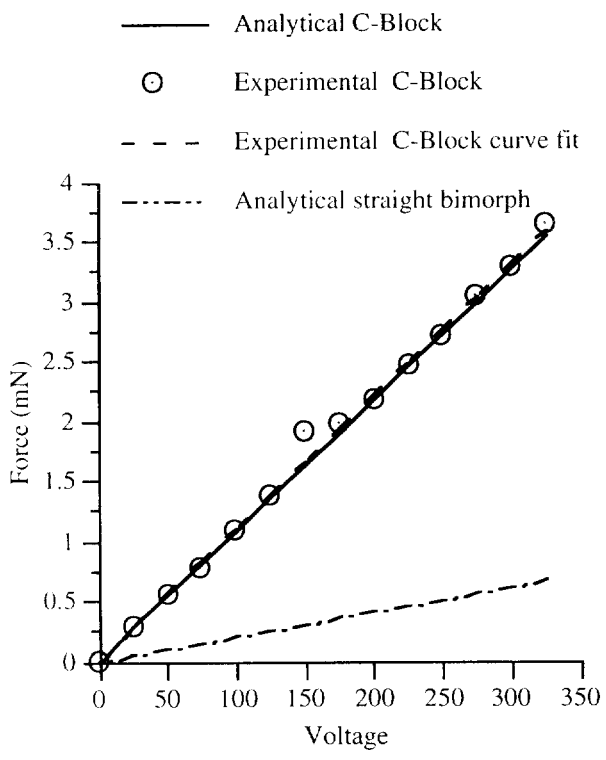

Figure 9. Single actuator; force versus voltage (r = 1.56 cm, t_{tot} = 0.148 mm).

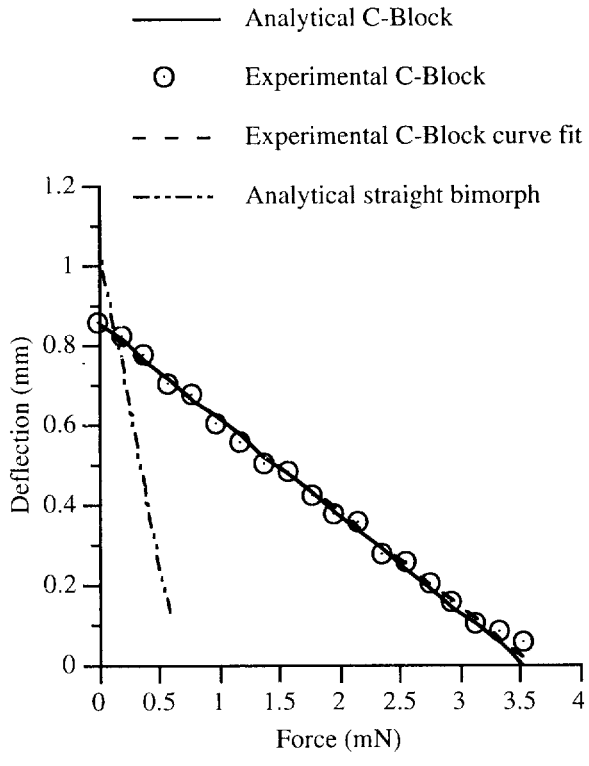

Figure 10. Single actuator; force versus deflection (r = 1.56 cm, t_{tot} = 0.148 mm).

guarantees that the total thickness is also less than the radius for a physically meaningful design. A single C-block actuator is permitted to curve only in one direction to avoid numerical problems caused by taking logarithms of negative numbers in the formulation of r_n as mandated by the sixth constraint, g_6. In many practical applications, actuators have strict length and height limitations. The seventh and eighth constraints (g_7 and g_8) represent length and height constraints, respectively, which are imposed to ensure that the macroactuator fits inside a specified volume. It is assumed that the maximum possible electric field is applied to the actuators without damage to or depolarization of the piezoelectric layers. Since the voltage required to maintain a constant electric field increases proportionately with the piezoelectric layer thickness, a constraint (g_9) is placed on the maximum applied voltage to ensure a practical design. Lower bounds on the thickness design variables are due to manufacturing limitations. Upper bounds are imposed to ensure a physically reasonable design. The bounds on the radius design variable are also justified in this manner. Side constraints on the discrete design variables are implied when the specific allowable values for each variable are specified. The material and other relevant properties are presented in Table 1 and additional parameters are presented in Table 2.

Table 1. Material properties.

Property	Value
Y_b (N/m^2)	1.9 x 10^9
Y_p (N/m^2)	5.4 x 10^9
Y_e (N/m^2)	7.0 x 10^8
d_{31} (m/V)	2.3 x 10^{-11}

Table 2. Miscellaneous parameters.

Parameter	Value
v_{max} (volts)	500
E_3 (V/m)	30.0 x 10^5
l_{max} (cm)	10.0
h_{max} (cm)	3.00

The results obtained using the hybrid optimization procedure are presented in Table 3 and in Figs. 11-14. Analytical gradients are calculated for the continuous design variables in the current work to reduce computational effort during optimization. A value of ρ=50 is used for the K-S function to ensure that no constraints are violated in the final design. The hybrid algorithm randomly selects a single design variable, either discrete or continuous, for each iteration. A step size of up to 1% for the continuous variables is found to be appropriate. The discrete variables can be selected from integer values within a range of ±10% of its current value. Significant improvements are obtained in all the objective functions while satisfying the constraints in the final design. The objective functions are presented, normalized with respect to their initial values, in Fig. 11. Note that the objective functions must be scaled to a log axis due to the dramatic improvements after optimization. For instance, the deflection Δy increases almost three orders of magnitude compared to the initial design. The respective dimensional values can be found in Table 3. A summary of the optimization results is also presented in Table 3 for the three different cases that are investigated. Design variables which are not relevant for a particular case and eliminated from the original set are held constant during optimization and are indicated in this table by ().

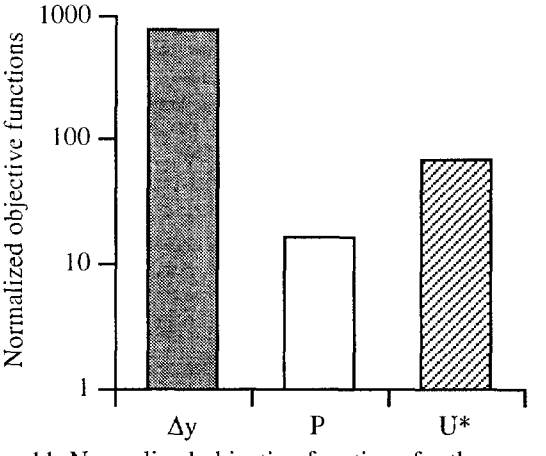

Figure 11. Normalized objective functions for three cases.

6.2. Case 1 Maximize deflection

In this case, the induced deflection of the actuator is maximized by minimizing f = - |Δy|. Since the deflection is independent of the number of units in parallel, p_{nu} is set equal to one and is eliminated from the set of design variables. Therefore, constraint g_7 assumes the following form.

$$\frac{2}{h}\left[r+\frac{t_{tol}}{2}\right]-1\le 0 \qquad (9)$$

As both r and s_{nu} increase, the deflection also increases. Since the length constraint is clearly active in the final design, the optimization problem can be simplified by using the length constraint (g_8) to determine r, thereby eliminating it as an independent design variable.

$$r=\frac{l_{max}}{2s_{nu}} \qquad (10)$$

The design variables corresponding to the three thicknesses, t_b, t_e and t_p, are all driven to their respective lower bounds during optimization. In the final design, snu=1, indicating that a single thin actuator with radius r =

$l_{max}/2$ maximizes the deflection. It was previously noted in Refs. 8 and 15 that for a single actuator, deflection is maximized by a thin, straight beam with a ratio t_p/t_{tot} = 0.4. This trend is also observed in the current optimization results where the ratio t_p/t_{tot} approaches 0.4 although the lower bound imposed on t_p is reached before this optimal ratio can be achieved. Additionally, the largest possible radius is obtained indicating the trend towards a straight beam for this case. Figure 12 presents the representative final design for displacement maximization. The volume constraints are also included in this figure as indicated by the box surrounding the C-block actuator. Note (Table 3) that the deflection is maximized at the expense of the force thus drastically reducing the available work done by the actuator.

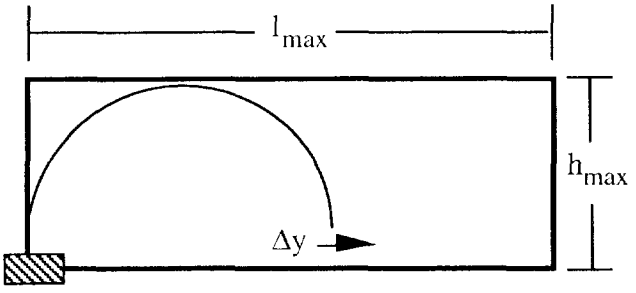

Figure 12. Single thin actuator to maximize deflection.

6.2. Case 2 - Maximize force

This case investigates force as the objective function which is maximized by minimizing f = - |P|. In this case, the force is independent of the number of units in series, s_{nu}. Therefore, its value is set equal to one and it is eliminated from the design variable vector. The results for this case are presented in Table 3 and Fig. 13. Although the height constraint (g_7)is active in the final design, it is not used to eliminate any design variables as in the previous case due to numerical problems which can develop during optimization such as attempts to take logarithms of negative numbers. The electrode layer thickness (t_e) decreases to its lower bound due to its lower modulus compared to the other layers present. The piezoelectric layer (t_p) increases until the voltage constraint is violated and the radius (r) decreases until its value reaches the total thickness of the actuator. The ratio t_p/t_{tot} is also near 0.4 as observed in previous work[8,15]. However, contrary to a previous finding[15] which showed that the bonding layer t_b increases to increase the moment arm which maximizes the force in a single actuator configuration, the present study shows that the bonding layer thickness (t_b) reduces to its lower bound while the number of units in parallel (p_{nu}) increases until the height constraint becomes active. This indicates that many thin curved beams acting in parallel represents a superior configuration than a single thick curved beam. Although the induced deflection is very small, note the large force of 25.4 N (Table 3) which develops from such a macroactuator configuration. The representative actuator which maximizes the force is shown in Fig. 13. Recall that the force is independent of the number of units in series (s_{nu}). Therefore, only a single unit in series is presented with many units in parallel.

Table 3. Optimization results.

Design variable	Initial	Final		
		Case 1 (Δy)	Case 2 (P)	Case 3 (U*)
t_b (μm)	10.0	5.00	5.00	5.00
t_e (μm)	10.0	0.60	0.60	0.60
t_p (μm)	10.0	8.00	16.2	16.7
r (mm)	0.10	15.0	0.04	0.19
t_p/t_{tot}	0.14	0.34	0.41	0.41
p_{nu}	100	(1)	752	722
s_{nu}	100	1	(1)	261
Δy (mm)	0.004	3.08	0	0.076
P (N)	1.52	0	25.41	5.50
U* (Nm)	3.84×10^{-6}	0	0	2.59×10^{-4}
v (volts)	300	240	486	500
t_{tot} (μm)	70.00	23.4	39.8	40.8

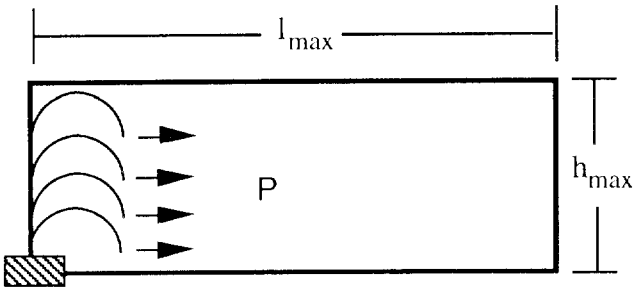

Figure 13. Multiple actuators in parallel to maximize force.

6.3. Case 3. - Maximize strain energy

It is desirable to create an actuator which can produce both deflection and force. Therefore, the induced strain energy (work) from piezoelectric actuation is maximized as an objective function by minimizing $f = -|U^*|$. Results for this case are presented in Table 3 and Fig. 14. The results indicate a trade-off between the those obtained through individual maximization of force and deflection. It is observed from Table 3 that the bonding layer and electrode layer thicknesses decrease to their respective lower bounds while the piezoelectric layer thickness increases until the voltage constraint became active. Again, the optimal ratio $t_p/t_{tot} = 0.4$ is obtained. The results agree with the optimal values obtained by Crawley and Anderson[15] for similar structures.

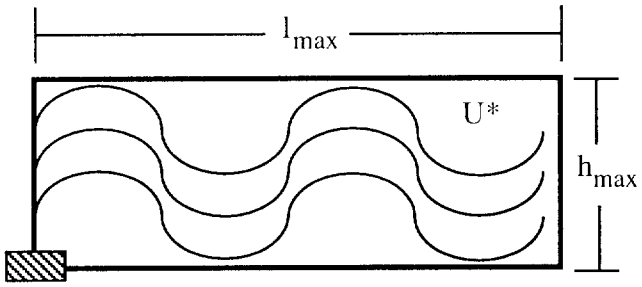

Figure 14. Multiple C-blocks in parallel and series to maximize strain energy.

Since the bonding layer thickness is driven to its lower bound, the number of units in parallel p_{nu} increases until the height constraint (g_7) becomes active. Since this constraint is active in the final design, there is a trade-off between a few thick actuators and many thin actuators to maximize U*. The intermediate value of the radius in the final design, compared to the first two cases, is also an indication of this trade-off. The hybrid optimization technique indicates that many thin actuators in parallel are superior to a few thick ones as shown in Fig. 14 to maximize the strain energy.

7. Concluding remarks

The piezoelectric material PVDF was used to construct a C-block type actuator. This microactuator was used as a building block to form macroactuators by combining multiple units in series and in parallel which gives significantly superior performance. Experimental validation of the mathematical model was provided. Since efficient design of these actuators involves various performance issues, an optimization technique was used to address this problem. The associated design variables were both continuous and discrete in nature. Therefore, a hybrid optimization technique was used based on a modified Simulated Annealing algorithm which also uses gradient information for improved efficiency. Deflection, force and strain energy were used as objective functions with constraints on geometry and voltage. The following important observations were made from this study.

1) Experimental tests conducted showed excellent agreement with the quantitative C-block actuator model development.

2) The hybrid optimization procedure significantly improved design objectives while satisfying all constraints.

3) The ratio of the piezoelectric layer to the total microactuator thickness approached 0.4 which was previously determined to be an optimal thickness ratio by other researchers.

4) A single thin C-block type actuator using PVDF piezoelectric film is best for maximizing induced deflection.

5) Multiple thin actuators combined in parallel with small radius are better for maximizing force.

6) Maximization of the strain energy results in an optimum configuration which shows a distinct trade-off between maximization of deflection and force separately. The optimum configuration comprises multiple thin actuators with many parallel and series units and an intermediate value of radius.

7) Since the C-block actuator configuration can provide more work than an equivalent straight bimorph actuator, it is a better design choice than the commonly used straight bimorphs.

8. Acknowledgments

This research was supported by the U.S. Army Research Office, Grant Number DAAH04-94-G-0157, Technical monitor, Dr. Gary Anderson.

9. References

1 Crawley, E. F. and de Luis, J. "Use of Piezoelectric Actuators as Elements of Intelligent Structures" *AIAA Journal*, Vol. 5, No. 10, Oct. 1987, pp. 1373-1385.

2 Heeg, J "Flutter Suppression via Piezoelectric Actuation" MS Thesis, George Washington University, August 1991.

3 Samak, D. K. and Chopra, I. "Design of High Force, High Displacement Actuators for Helicopter Rotors" *Proc.* SPIE North American Conference on Smart Structures and Materials, Orlando, FL, Feb. 14-16, 1994, pp. 86-89.

4 Chen, P. C. and Chopra, I. "Induced Strain Actuation of Composite Beams and Rotor Blades with Embedded Piezoceramic Elements" SPIE North American Conference on Smart Structures and Materials, Orlando, FL, Feb. 14-16, 1994, pp. 123-140.

5 Thirupathi, S. R. and Naganathan, G. G "Use of Piezoceramic Actuator For Automotive Active Suspension Mechanisms: A Feasibility Study" *Proc.* 22nd Biennial Mechanism Conference, Scottsdale AZ, Sept. 23-26, 1992, pp. 233-241.

6 Baz., A. and Poh "Performance of an Active Control System with Piezoelectric Actuators" *Journal of Sound and Vibration*, Vol. 126, No. 2, 1988, pp. 327-343.

7 Brei, D. "Design and Development of a New Class of Piezoelectric Actuators for Force Improvement" *Proc* Society of Engineering Science 31st Annual Technical Meeting, College Station TX, Oct. 10-12, 1994.

8 Brei, D. "Design and Development of a Piezoelectric Microactuator Building Block for Deflection Improvement" *Proc.* Symposium on Micro-Mechanical Systems, ASME Winter Annual Meeting, Chicago IL, Vol. 2., Nov. 6-11, 1994, pp. 717-723.

9 Vanderplaats, G. N. *Numerical Optimization Techniques for Engineering Design with Applications*, McGraw-Hill Publishing Company, New York NY,1984.

10 Onoda, J. and Hanawa, Y. "Optimal Locations of Actuators for Statistical Static Shape Control of Large Space Structures: A Comparison of Approaches" *Proc.* of the 33rd AIAA/ASME/ASCE/AHS/ASC Structures, Structural Dynamics and Materials Conference, Dallas, Tx., Apr. 13-15, 1992, pp. 2788-2795.

11 Goldberg, D. E., *Genetic Algorithms in Search, Optimization and Machine Learning*, Addison Wesley Publishing Company, New York NY, 1989.

12 Chattopadhyay, A. and Seeley, C. E. "Development of a Hybrid Optimization Technique with Application to Buckling of Cylindrical Shells" *Proc.* WCSMO-1, The First World Congress of Structural and Multidisciplinary Optimization, Goslar, Lower Saxony, Germany, May 28-June 2, 1995.

13 Kirkpatrick, S., Gelatt, C. D. Jr., Vecchi, M. P. (1983) "Optimization by Simulated Annealing" *Science* Vol. 220, No. 4598, May, 671- 680.

14 Lombardi, M., Haftka, R. T. Cinquini, C. "Optimization of Composite Plates of Buckling by Simulated Annealing" *Proc.* 31st AIAA/ASME/ASCE/AHS/ASC Structures, Structural Dynamics and Materials Conference, Dallas Tx., April 13-15, 1992, pp. 2552-2562.

15 Crawley, E. F. and Anderson, E. H. "Detailed Models of Piezoelectric Actuation of Beams" *Proc.* of the 30th AIAA/ASME/ASCE/AHS/ASC Structures, Structural Dynamics and Materials Conference, Mobile, Al., April 1989, pp. 2000-2010.

16 Kreisselmeir, G. and Steinhauser, R. "Systematic Control Design by Optimizing a Vector Performance Index" *Proc.* International Federation of Active Controls Symposium on Computer-Aided Design of Control Systems, Zurich, Switzerland, Aug. 29-31, 1979, pp.107-113.

17 Seeley, C. E. and Chattopadhyay, A. "A Simulated Annealing Technique for Multiobjective Optimization of Intelligent Structures" *Smart Materials and Structures*, Vol. 3, 1994, pp. 98-106.

18 Anderson, E. H. and Hagood, N. W. "A Method for Improving Randomized Search Placement Algorithms" *Proc.* SPIE North American Conference on Smart Materials and Structures, February 12-17, 1994, pp 308-322.

19. H.S. Tzou "Development of a Lightweight Robotic End Effector Using Polymeric Piezoelectric Bimorph" *IEEE Conference on Robotics and Automation*, pp. 1704-1709, 1989.

20. W.W. Hines and D.C. Montgomery, *Probability and Statistic in Engineering and Management Science*, John Wiley and Sons, New York, New York, pp. 262-306, 1990.